2013

EXAFS and EPR analysis of the local structure of Mn-doped $Li_2B_4O_7$

T D. Kelly
Air Force Institute of Technology

L Kong
University of Nebraska-Lincoln

D A. Buchanan
Air Force Institute of Technology

A T. Brant
Air Force Institute of Technology

J. C. Petrosky
Air Force Institute of Technology, James.Petrosky@afit.edu

See next page for additional authors

Authors

T D. Kelly, L Kong, D A. Buchanan, A T. Brant, J. C. Petrosky, J W. McClory, V T. Adamiv, Y V. Burak, and Peter A. Dowben

EXAFS and EPR analysis of the local structure of Mn-doped Li₂B₄O₇

T. D. Kelly*,¹, L. Kong², D. A. Buchanan¹, A. T. Brant¹, J. C. Petrosky**,¹, J. W. McClory¹, V. T. Adamiv³, Y. V. Burak³, and P. A. Dowben²

¹ Department of Engineering Physics, Air Force Institute of Technology, 2950 Hobson Way, WPAFB, OH 45433, USA
² Department of Physics and Astronomy and the Nebraska Center for Materials and Nanoscience, Theodore Jorgensen Hall, 855 North 16th Street, University of Nebraska-Lincoln, Lincoln, NE 68588-0299, USA
³ Institute of Physical Optics, 23 Dragomanov Street, Lviv 79005, Ukraine

* Corresponding author: e-mail tony.kelly@afit.edu, Phone: +1 937 255 3636, ext. 7300, Fax: +1 937 904 8022
** e-mail petrosky@afit.edu, Phone: +1 937 255 3636, ext. 4562, Fax: +1 937 904 8022

The local structure of Mn-doped Li₂B₄O₇(001) was investigated using extended X-ray absorption fine structure (EXAFS) at the Mn K edge and electron paramagnetic resonance (EPR). The location of the Mn dopant in a lithium tetraborate crystal is consistent with occupation of a site with strong oxygen coordination. The Mn–O bond lengths are similar to those observed with Mn doping of the icosahedral based boron carbide where Mn is in a substitutional dopant in one of the cage sites. From EXAFS, the manganese does not appear to greatly alter the overall tetragonal form of lithium tetraborate, with the dopant most likely substituting for one of the two B sites and with placement of some of the Mn in a Li site still possible. The EPR spectra agree with the literature examined resolving multiple Mn species in the crystal lattice.

© 2013 WILEY-VCH Verlag GmbH & Co. KGaA, Weinheim

1 Introduction As illustrated in Fig. 1, the oxide lithium tetraborate ($I4_1cd$, $a = 9.479$ Å, $c = 10.290$ Å) is a complex tetragonal crystal with 104 atoms in a unit cell [1–5]. The pyroelectric and piezoelectric properties of the lithium borates require excellent dielectric properties [6] in the crystals of Li₂B₄O₇, particularly along the polar [001] direction. This material has been measured to have undoped resistivity of 10^{10} Ω cm or more [7, 8]; consequently, for applications such as scintillation or use in solid state devices, doping of lithium tetraborate may be essential. For example, in semiconducting boron carbides the resistivity problem has been circumvented by filling impurity bands [9, 10]. This appears to lead to dramatic increases in carrier concentrations in materials with otherwise very large carrier effective masses [10]. Similarly, carrier mobility and carrier concentrations both may be increased in lithium tetraborates by the addition of impurities [6, 7]. Lithium borates [8, 11–13] are among the boron rich materials (e.g., BN [14–16], BP [17–20], and BC [21–29]) that have been considered as possible materials for effective solid state neutron detectors.

Applying extended X-ray absorption fine structure (EXAFS) techniques to successfully determine the physical structure of the *undoped* lithium tetraborate is unlikely due to the low boron and oxygen K-shell X-ray cross-sections [30–31]. However, with transition metal doping the local structure, in the vicinity of the transition metal, is accessible and an EXAFS analysis is a comparatively useful technique [30–31]. Among the boron rich, low Z materials, boron carbide has also been Mn doped [31]. It was found that Mn occupies the apical site as a substitution in an icosahedral cage site and a local antiferromagnetic ordering is believed to be favored [32] in the pairwise doping that occurs on adjacent icosahedra. The present research investigates whether Mn doping in a boron rich carbide can be compared to the Mn doping of a boron rich oxide.

2 Experimental The Mn K-edge EXAFS spectra were collected at the DCM beamline at the Center for Advanced Microstructures and Devices (CAMD). Monochromatic light was obtained using a double crystal monochromator of the Lemonnier type [33], equipped with a Ge (220) crystal pair. The energy resolution was approximately 2 eV. Spectra were collected in the fluorescence yield mode using a Canberra 13-element high purity
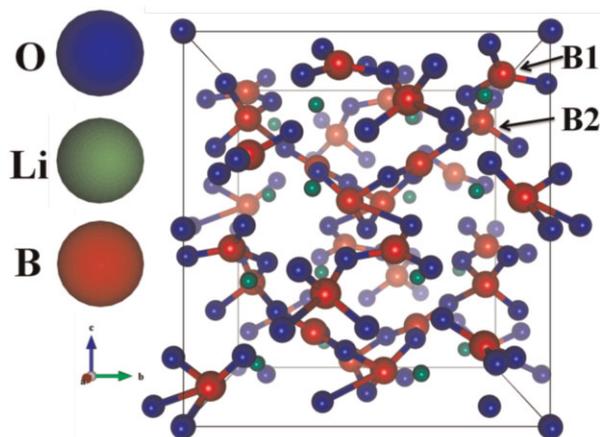
Phys. Status Solidi B 250, No. 7 (2013)

1377

Original

Paper

Figure 1 (online color at: www.pss-b.com) Model of the undoped lithium tetraborate crystal: oxygen – blue, boron – red, lithium – green. Labeled are the B1 and B2 sites, where the latter correspond to BO_3 and BO_4 structures, respectively.

germanium diode array detector. Due to the low transition metal concentrations, the data were not corrected for self-absorption. The absolute energy scale was calibrated by assigning the established K-edge to the first inflection point of the spectra taken from the appropriate metal foil. The EXAFS data were reduced by following standard procedures [34], and analyzed by the FEFF-6 codes, as done previously with the Mn doped boron carbides [31]. The oscillatory photo-absorption cross-section (K-shell excitation) is roughly:

$$\chi(k) = \frac{|f(k,\theta)|}{k} \sum_i W_i \sin[2kR_i + \alpha(k)] \\ \times \exp(-\gamma R_i - 2\sigma_i^2 k^2), \tag{1}$$

where $f(k,\theta)$ is the atomic scattering factor, and the weight from the atoms in each shell radius, i, due to the manganese is given in terms of W_i.

W_i is the overall amplitude or weight of a scattering path, which is often labeled as $N * S_o^2$ where the summation is over coordination shells so that N is the coordination number and then S_o^2 is the passive electron amplitude reduction factor, which accounts for many-electron excitations. In this paper we label it as a single term to emphasize the form of χ. W_i and γ (also called $1/\lambda$, inverse mean free path of the photoelectron) explain why EXAFS is a short order theory and why the EXAFS oscillations decay at large wave numbers.

In a similar way, the term $\alpha(k)$ is the combination of the two phase shifting parameters. As the photoelectron leaves the absorbing atom, it shifts by δ_{absorb} and travels kR_i to the neighboring atom. As it scatters, it is also phase shifted by $\varphi_{neighbor}$. The wave then travels back to the absorbing atom for another kR_i and experiences the δ_{absorb} once again, $\alpha(k) = 2\,\delta_{absorb} + \varphi_{neighbor}$. σ^2 is usually referred to as the *Debye–Waller factor* as it accounts for mean-squared deviations in the distance R_i. A typical experimental $\chi(k)$ spectrum weighted by k demonstrates good data quality up to $\sim$10–15 Å^{-1} depending on the material.

The Mn doped lithium tetraborate ($Li_2B_4O_7$:Mn) single crystals, with the natural isotope abundance (^{6}Li – 7.4%, ^{7}Li – 92.6%, ^{10}B – 19%, ^{11}B – 81%, and ^{55}Mn – 100%), were grown from the melt by the Czochralski technique as described elsewhere [11, 35, 36]. In the growth process of the $Li_2B_4O_7$:Mn, MnO_2 was added into the $Li_2B_4O_7$ melt at a 0.4% molar concentration. The single crystal $Li_2B_4O_7$:Mn samples are nominally $Li_{1.95}Mn_{0.05}B_4O_7$, as determined by quantitative spectrographic analysis. The manganese appears to reduce from Mn^{4+} to Mn^{2+}, bivalent in the $Li_2B_4O_7$:Mn lattice. All other impurities amount to <0.05%, with the principal impurity being Cu. The major crystal defects, however, are not impurities but vacancies.

3 Results Plotted in Fig. 2 is the entire Mn K-edge absorption spectra, including the X-ray absorption near edge tructure (XANES) and EXAFS for $Li_2B_4O_7$(001):Mn. The graph extends from approximately 150 eV below the Mn K-edge to nearly 1000 eV above, and the characteristic signature of manganese is evident with the Mn K-edge determined to be at values close to the expected [37, 38] Mn K-edge (E_F–E_K), at 6539 eV. The Mn K-edge (E_F–E_K) for lithium tetraborate, at 6547 eV, is consistent with the approximate 9–10 eV wide band gap of $Li_2B_4O_7$ [6, 39–42]. The smaller 0.7 eV band gap of semiconducting boron carbide [43, 44], has little influence on the position of the Mn K-edge, as seen in Fig. 2.
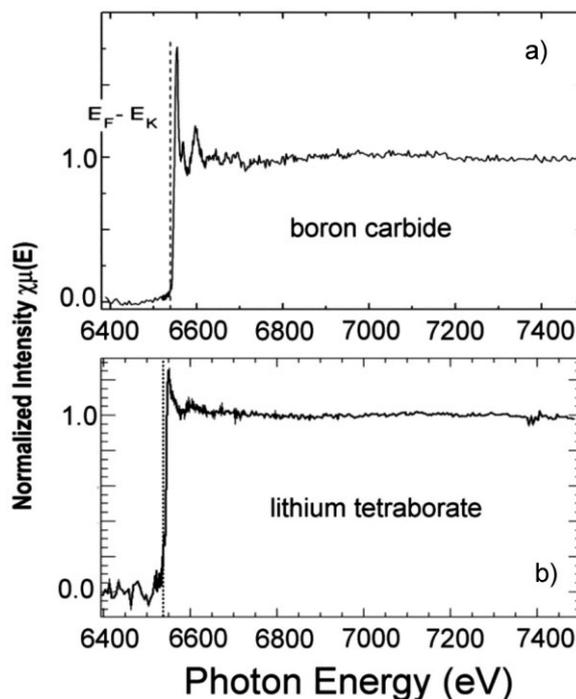

Figure 2 The normalized Mn K-edge XANES spectra of (a) Mn doped PECVD semiconducting boron carbides and (b) crystalline lithium tetraborate $Li_2B_4O_7$(001). The Mn K-edge energy (E_F–E_K) at 6539 eV is seen for Mn doped boron carbide and 6547 eV for Mn doped lithium tetraborate.

In Fig. 2b, features similar to typical MnO powder Mn K-edge absorption spectra are found the pre-edge (small, dark peak to the left of dotted line at 6547 eV) and XANES region (as in Ref. [45]), offering further evidence of the presence of a Mn dopant in this $Li_2B_4O_7$(001):Mn material. The presence of the pre-edge feature, commonly found in XANES spectra of the transition metals [45], is indicative of crystal symmetry under inversion operations and may suggest that the tetrahedral crystal symmetry is retained and that the manganese is dominated by nominally Mn^{2+}, but a mixed valence Mn remains possible.

3.1 Local structure from EXAFS It is assumed that the Mn introduced into the lithium tetraborate crystal does not greatly alter the overall tetragonal form; furthermore, Mn coordinated by oxygen seems to be the most likely configuration. The presence of the Mn dopant contributes to an underlying X-ray absorption fine structure oscillation, most notably between approximately 3 and 11 $Å^{-1}$. After background subtraction and application of the Fourier transformation, the coordination shell distances are extracted as shown in Fig. 3. While the magnitude of the Fourier transformed $k\chi(k)$ is not precisely the pair radial distribution function, this provides an indication of the radial spacing of atoms in the vicinity of Mn. Since the entire k-range was not used in this analysis, and given the complexity of the crystal structure, and also the known issues related to the weak X-ray scattering factors common to oxygen, lithium, and boron, only the first few coordination shell distances may be reliably examined. The significance of the low-Z cross-section is reduced because the region of the radial distribution function of greatest interest is the first coordination shell, corresponding to radial distances of 1.0–2.4 Å from the Mn impurity. The first peak at ∼0.8–2 Å relates primarily to a single-scattering contribution of Mn–O pairs. The results in the region of the first shell closely resemble MnO (Fig. 3) and
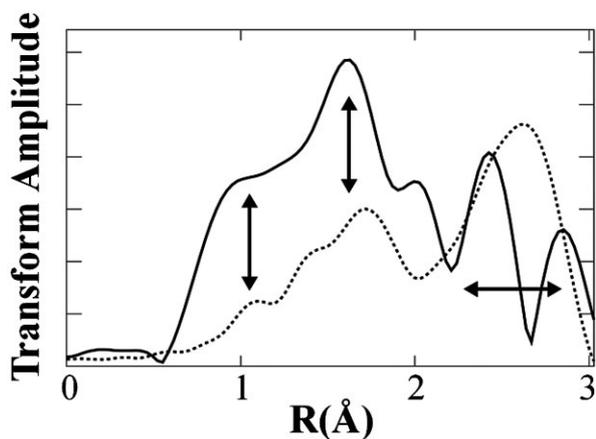
suggest that MnO bonds are similar to the Mn–O bonds in lithium tetraborate.

There are several circumstances to consider: (1) Mn supplants Li, (2) Mn substitutes B; of which there are two sites B1 and B2 (BO_3 and BO_4 respectively), (3) Mn is interstitial, or (4) Mn is in multiple valence states and forms a combination of 1, 2, and/or 3. The corresponding structure and elemental sites are shown in Fig. 1. Initial model calculations (Fig. 4) show that the scattering paths for Mn in the B1 sites as compared to the B2 sites were largely indistinguishable, suggesting that Mn could replace boron atoms in both the B1 and B2 sites, or that if there is a preferential boron site, this cannot be uniquely determined from the data presented here. Consequently, the comparison of the theoretical calculations for the different substitutional sites to the experimental data allows placement of the manganese at either boron site location, as indicated by the experimental fitting in Fig. 4. In Fig. 4, only single scattering paths were considered in the calculation. It is also possible that the Mn dopes by occupying the lithium site, but occupation of lithium sites alone is not consistent with the results (as discussed below).

As shown in Fig. 4, part of the Fourier transform of the EXAFS data places the first broad peak of the absorbance versus radius at about 1 Å. Considering that the inter-atomic spacings in the crystal are expected to be greater than 1 Å,
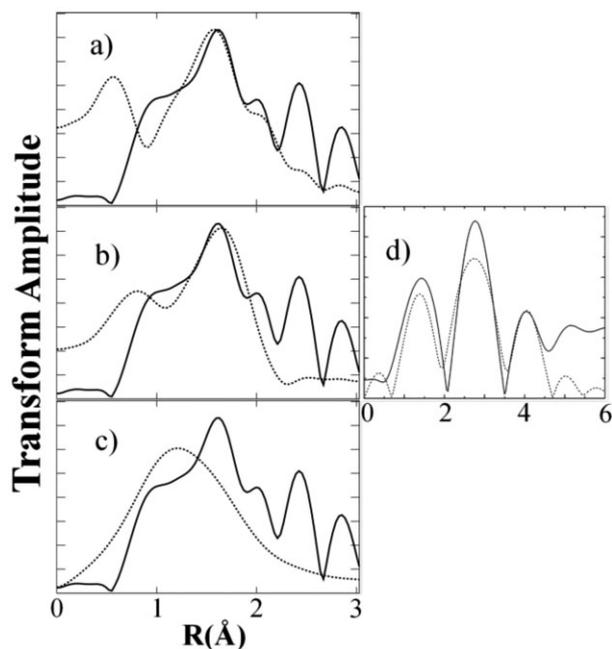

Figure 4 The magnitude of the Fourier transformed EXAFS $k\chi(k)$ data for the manganese doped lithium tetraborate (experiment solid line) are compared with the theoretical Fourier transformed EXAFS $k\chi(k)$ (broken lines) for Mn placed in the (a) B1 or (b) B2 boron sites, and sitting in the (c) lithium substitutional site. The spectrum is fit from 1 to 2.4 Å, though the figure shows data up to 3.0 Å. The data are transformed from the data taken from the XANES edge up to 11.0 $Å^{-1}$. For reference, the $B_{12}C_2$:Mn results are shown in (d).

Figure 3 Magnitude of the Fourier transformed EXAFS $k\chi(k)$ data for the manganese oxide MnO (dotted line) adapted from Ref. [46] and manganese in $Li_2B_4O_7$ (solid line). The data are transformed from data taken between 2.4 and 11.0 $Å^{-1}$.

Phys. Status Solidi B 250, No. 7 (2013)

Original
Paper

1379

this contribution is most likely due to a XANES feature similar to that attributed to MnO bonds ([46] for example), as shown in Fig. 3.

The first coordination shell consists of oxygen atoms, whether Mn is in the B1 site of the BO_3 clusters, the B2 site of the BO_4 clusters, or the Li tetrahedral; and this is consistent with the expectations obtained by experiment. All such oxygen coordination sites form tight bonds that could contribute to the XANES structure. Because of the low Mn concentration, Mn will only occupy a minute fraction of the B1 (or B2) sites, and conceivably some Li sites. Consequently, accurate modeling of Mn doped lithium tetraborate would require an exceptionally large unit cell. Realistic, more tractable modeling of the EXAFS data uses cluster sizes that are smaller than would be the case for a more accurate description, causing the Mn scattering to be over-weighted. In spite of these difficulties, the experimental data is fit exceedingly well (Fig. 4).

Since distinguishing between the B1 and B2 substitutional doping was not possible, leaving two best fits as shown in Fig. 4a, b. Either Mn substitutional placement causes a stretch in the bonding lengths at the B1 site and a contraction at the B2 site or vice versa. In both situations, the resulting fit parameters are nearly the same. However, the contraction will be more pronounced for one of the two B sites, which could be due to the sub-cluster structures within the unit cell (Fig. 1).

If the manganese substitutes into a Li site, the contraction of the local lattice would be significant and would not, by itself, be surprising as this allows for tighter bonds to be formed between the transition metal and nearby neighbors, particularly the oxygen atoms. However, this placement might cause a large distortion of the lattice in the immediate vicinity of the lithium site. The observed features at smaller radii in the experimentally derived radial distribution function are poorly described by the absorbance-versus-radius generated by various cluster models and the fit is unlikely, as shown in Fig. 4c. The number and placement of theoretical absorption peaks, with radius, for substitution Mn in a Li site in the $Li_2B_4O_7$ lattice makes it unlikely that a Li substitution *alone* occurs within the lattice. Whereas, a Mn substitution for either B site in the $Li_2B_4O_7$ lattice has the correct number of absorption peaks with radius and the correct placement with only the relative amplitudes skewed.

3.2 Local structure from electron paramagnetic resonance (EPR) EPR is a technique for studying chemical species that have one or more unpaired electrons. Prior EPR [48–50] and optical [47, 49, 51–53] investigations of the doped $Li_2B_4O_7$:Mn single crystals and glasses have been interpreted as Mn entering the $Li_2B_4O_7$ lattice as Mn^{2+} ions, and into the $Li_2B_4O_7$ glass structure in the form of Mn^{2+} and Mn^{3+}. In prior work, it has been suggested that the Mn dopant takes the place of Li^+ in a deformed tetrahedral oxygen environment. This doping site would make Mn doping very similar to that of Ag [54], but the luminescence data for Mn dopants' X-ray luminescence [47, 55] and EPR

[49] suggests that the role of Mn is quite different from Cu and Ag as a dopant in the $Li_2B_4O_7$ lattice, and possibly reflects either a multivalent Mn or Mn occupying multiple sites within the lattice.

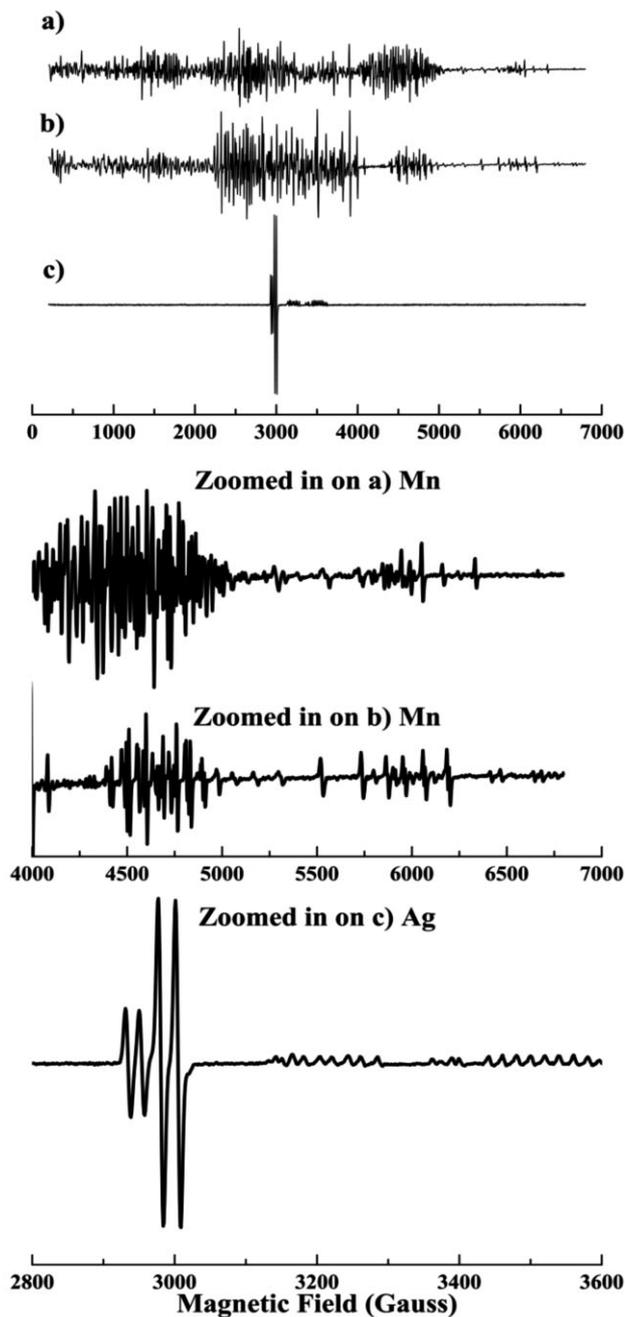The EPR transitions shown in Fig. 5 for $Li_2B_4O_7$:Mn single crystals (taken at 25 K) are sharper than most

Figure 5 The EPR spectrum from $Li_2B_4O_7$ with (a,b) Mn and (c) Ag doping. The EPR features are seen to be extremely sensitive to orientation. The spectra were taken with orientation for the $Li_2B_4O_7$:Mn crystal (a) roughly along the (001) direction and (b) orthogonal to the (001) direction, while the orientation for the Ag doped $Li_2B_4O_7$ crystal (c) is along the (001) *c*-axis direction.

previously reported [47, 48], bearing some resemblance to the results of Ref. [49]. In Ref. [49], a room temperature EPR spectrum was plotted for Li$_2$B$_4$O$_7$:Mn. In the spectrum of Ref. [49] there are six lines identified between approximately 6000 and 6500 G and then again from 6500 to 7000 G. In the middle subfigure of Fig. 5, the EPR spectrum for Mn is magnified in this region, showing similar features, although shifted by approximately 700 G. These EPR spectra are very sensitive to the crystallographic orientation, which may explain the difference, as the EPR features have an observable shift with even a 1/2 degree of magnetic field rotation.

Even so, the EPR spectra alone do not provide sufficient spectral sensitivity to determine the exact nature of the Mn location. However, when compared to other references, *e.g.* [50], some theory on the local environment can be established. The sensitivity and interpretability of the EPR spectra for Mn doped Li$_2$B$_4$O$_7$ in (a) and (b) of Fig. 5 can be compared to (c) for the Ag doped crystal. The latter is a cleaner sample to analyze because of the reduced spectral features; leading to easier interpretation of the EPR [54]. Neutral Mn has an electronic configuration of [Ar]3d^{5}4s^2, resulting in a partially filled d-shell for most accessible charged states. In particular, Mn^{2+} is in a high spin state with 5 unpaired electrons in its valence shell (S = 5/2), with nuclear spin I = 5/2. This alone should produce 5 sets of 6 EPR lines of equal intensity, one of which we identified earlier between 5500 and 6250 G (Fig. 5).

In Fig. 5c, the more simple EPR spectrum of Ag doped lithium tetraborate is plotted. Two pairs of sharp lines show the Ag^{2+} occupation of a Li site. However, of particular interest are the much weaker but notable Ag^0 lines from 3100 to 3600 G. This portion of the EPR spectrum is interpreted as Ag^0 atoms doping interstitially, but near enough to B atoms to interact [54]. When considering the Mn doped spectra, particularly between 4000 and 5500 G (Fig. 5a), many more lines are found than the expected $6 \times 5 = 30$ from hyperfine structure. Weak hyperfine interactions with nearby boron nuclei would further split each manganese hyperfine line into additional lines, resulting in a very complicated EPR spectrum. When compared with the literature, some other studies have proposed two different Mn sites in the lattice as well [50, 56]. In Ref. [50], two different Mn lines are observed, one interpreted as substituting in the Li site and the other as a B replacement in the tetrahedral site. In Ref. [56], two sets of Mn lines are noted, and it is suggested that the Mn^{2+} ion is in two different positions, each resulting in EPR lines. While we cannot clearly identify two EPR spectra, we do see more lines than expected for a Mn^{2+} ion at a Li$^+$ site, which could be similar to the multiple site occupations as with Ag doping of lithium tetraborate. In this situation, our EPR data suggests that in addition to a Li substitution, another Mn could be substitutionally located at a B site, as suggested by [50], or interstitially near a B site.

Although by no means conclusive, it has been suggested that the Mn dopant occupies a Mn^{2+} site in Li$_2$B$_4$O$_7$:Mn crystals, taking the place of B^{3+} in a tetrahedral structure [49,

57] or possibly as a Mn^{3+} interstitial [49], as well as, occupying Li$^+$ sites. This is consistent with the EXAFS data presented here.

4 Discussion

4.1 Comparing Mn dopant sites
When considering an impurity like Mn in the Li$_2$B$_4$O$_7$ crystal, one can start by comparing the ionic radii of corresponding ions and interatomic distances between the pertinent ions in the lattice. The ionic radii and valences in the Li$_2$B$_4$O$_7$ crystal, Li$^+$ (0.68 Å), B (0.20 Å), and O^{2-} (1.32 Å), suggest that the most favored tetragonal site is, in fact, the lithium site for all possible valences of manganese: Mn^{2+} (0.91 Å), Mn^{3+} (0.70 Å), Mn^{4+} (0.52 Å), Mn^{7+} (0.46 Å), although it is known that the most stable valence states for Mn should be 2, 4, and 7.

In the Li$_2$B$_4$O$_7$ structure, there are B^{3+} ions in both a trigonal position (B^{3+} in an environment of three O^{2-}) and a tetrahedral position (B^{3+} surrounded by four O^{2-}). The standard tetraborate boron–oxygen complex [B$_4$O$_9$]$^{6-}$ consists of two BO$_3$ and two BO$_4$ molecules. Consider the trigonal complex BO$_3$. The interatomic distances [4] are:

(i)   B(1)–O(1) = 1.355 Å
(ii)   B(1)–O(2) = 1.371 Å
(iii)   B(1)–O(3) = 1.374 Å,

so that in the BO$_3$ complex, the average distance is of the order of 1.367 Å. The expected geometrical distance, based on the sum of the ionic radii is B^{3+}–O^{2-} is of order 1.52 Å, so that the differences between expected geometrical distance and average real distance (based on the undoped Li$_2$B$_4$O$_7$ structure) is 0.153 Å. This is shorter than would be expected for Mn^{2+}, without significant strain, as the geometrical distance from Mn^{2+} to O^{2-} is about 2.23 Å, based on the ionic radii. The difference between expected geometrical distances based on ionic radii and real lattice spacing is now much larger: 0.863 Å. Even if we take into account the shortening of the bonds because of the covalence, it is still unlikely that Mn^{2+} will replace boron in the BO$_3$ trigonal complex.

Now consider the tetragonal complex BO$_4$. The interatomic distances in lithium tetraborate [4] are:

(i)   B(2) – O(1) = 1.453 Å
(ii)   B(2) – O(2) = 1.506 Å
(iii)   B(2) – O(3) = 1.506 Å
(iv)   B(2) – O(4) = 1.454 Å,

so that the average distance is ∼1.48 Å. The expected geometrical difference between B^{3+}–O^{2-} is again 1.52 Å, and the difference of the bond length based on ionic radii from the average experimental lattice spacing is small, 0.04 Å. Thus, the expected distance, based on ionic radii, is close to the experimental value in the BO$_4$ complex (1.48 Å). This is, however, much smaller than what is expected for Mn^{2+}–O^{2-} (2.23 Å); a fit into this lattice site would be difficult based on

ionic radius arguments alone. Based on the EXAFS results of Figs. 3 and 4, it may be possible to place the Mn^{2+} ion into either a B^{3+} trigonal or tetragonal site, so that there is some local strain of the lattice. In fact, the fits for Fig. 4 were the result of straining the lattice through a contraction of one complex and expansion of the other, suggesting such a strain is probable. However, as discussed next, this is hardly compelling.

The Li polyhedron represents a better fit based on the accepted ionic radii. The first coordination sphere (oxygen) Li^+ includes approximately four O^{2-} ions, which form a strongly deformed tetrahedron. The bond length distances are:

(i) $Li^+ - O(1) = 2.17$ Å
(ii) $Li^+ - O(2) = 1.967$ Å
(iii) $Li^+ - O(3') = 2.027$ Å
(iv) $Li^+ - O(3'') = 2.080$ Å,

resulting in an average distance of 2.061 Å for the first coordination sphere. This is closer to the expected geometrical distance for Mn of 2.23 Å. The next O^{2-} ion is positioned at 2.61 Å forming the fifth vertex of the Li polyhedron and forming the second coordination shell with seven oxygen atoms ranging in distances of 2.695–2.951 Å.

This is larger than the distance extracted from the EXAFS data, although qualitatively, the Mn EXAFS spectra for Mn in $Li_2B_4O_7$ are similar to that observed for Mn in MnO (Fig. 3). Thus, placement of a Mn dopant in the Li^+ position cannot be excluded. But based on the EXAFS data, if Mn substitutes Li exclusively, it would severely strain the bonds at these sites.

4.2 Comparing to $B_{12}C_6$:Mn Substitution of single-charged Li^+ by Mn^{2+} could occur and the charge imbalance may be compensated with the addition of Li vacancies. A bond length between 2.061 and 2.23 Å is expected when a Mn atom is in a Li site. This is close to the values calculated for 3d transition metal dopants in substitutional sites in semiconducting boron carbide [31]. Because of the significant number of charge redistributions possible, the EXAFS derived shell spacings may be much smaller than the actual atomic spacing; similar to the EXAFS measurements of transition metal dopants in semiconducting boron carbides. While tetrahedral coordination of the Mn placed in the lithium tetraborate lattice remains likely based on the EXAFS data, site determination is not definitive from EXAFS alone, as discussed above.

5 Conclusions The experimental data show that manganese is added successfully as a dopant in $Li_2B_4O_7$ and the XANES features are characteristic of MnO bonds. Analyses of the experimental data show that manganese atoms likely substitute at boron sites, but occupation of the lithium site is neither disproved nor excluded. In the former (B) sites, the local bonds are severely strained and in the latter (Li) case, the data would support a model that involves large charge redistribution.

These bonds are more contracted than the initial boron atomic bonds and much contracted from what is expected based on the ionic radii alone. The Mn doping of lithium tetraborate strongly resembles that of Mn doping of semiconducting boron carbide [31], but no evidence of pairwise doping of Mn is evident. The Mn K-shell near edge structure is strongly influenced by the fact that lithium tetraborate is a wide band gap insulator. These results, in the region of the first shell, closely resemble MnO and Mn doped boron carbide and suggests that Mn–B bonds in boron carbide are similar to the Mn–O bonds in lithium tetraborate.

The results of the EXAFS experiment suggest a Mn substitution in the boron site or interstitially and near to a B site (Fig. 6). This is supported in the literature from both EPR and luminescence measurements [50, 55, 56, 58, 59]. In the EPR papers, it has been shown there are two different Mn doping sites within the lithium tetraborate lattice, and while one has fourfold coordination with the nearest O atoms, the other has a higher coordination and substitutes for the tetrahedral B site. The EPR measurements presented in this paper confirm two possible Mn species. Based upon a similar analyses with $Li_2B_4O_7$:Ag, Mn may also occupy a B site, or at least interstitially very near a B atom.

When compared to photoluminescence in the literature, there are two species of Mn which contribute to two emission bands around 500 and 600 nm. The photoluminescence literature further postulates the presence of multiple charge states of Mn, which could also explain Mn substitutionally occupying multiple sites within the tetraborate structure. This cannot be effectively confirmed by EXAFS, though a future XANES analysis could shed more light on both the Mn valence and the amount of each valence present.
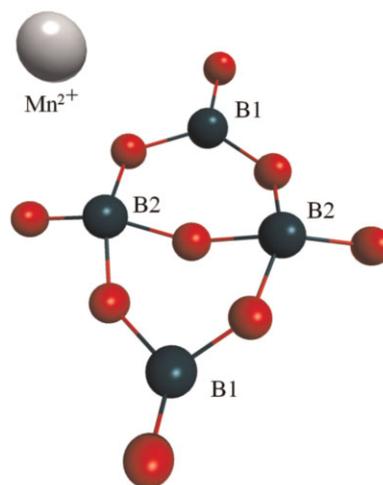

Figure 6 (online color at: www.pss-b.com) The primary building block element of the lithium tetraborate structure, adapted from Ref. [41]. The B1 (trigonal) and B2 (tetrahedral) sites are indicated as from Fig. 1. The figure is merely for demonstration of the B1 and B2 sites that are considered for Mn substitution.

References

[1] J. Krogh-Moe, Acta Crystallogr. **15**, 190 (1962).

[2] J. Krogh-Moe, Acta Crystallogr. B **24**, 179 (1968).

[3] M. Natarajan, R. Faggiani, and I. O. Brown, Cryst. Struct. Commun. **8**, 367 (1979).

[4] S. F. Radaev, L. A. Muradyan, L. F. Malakhova, Ya. V. Burak, and V. I. Simonov, Kristallografiya **34**, 1400 (1989).

[5] Ya. V. Burak, B. V. Padlyak, and V. M. Shevel, Radiat. Eff. Defects Solids **157**, 1101 (2002).

[6] V. T. Adamiv, Ya. V. Burak, D. Wooten, J. McClory, J. Petrosky, I. Ketsman, Jie Xiao, Ya. B. Losovyj, and P. A. Dowben, Materials **3**, 4550 (2010).

[7] C. Kim, B. Jun, H. Baek, D. Kim, Y. Hwang, H. Kim, G. Jeen, and J. N. Kim, J. Korean Phys. Soc. **4**, S10382 (2003).

[8] Sangeeta, K. Chennakesavulu, D. G. Desai, S. C. Sabharwal, M. Alex, and M. D. Ghodgaonkar, Nucl. Instrum. Methods Phys. Res. A **571**, 699 (2007).

[9] H. Werheit, J. Phys.: Condens. Matter **18**, 10655 (2006).

[10] H. Werheit, J. Phys.: Condens. Matter **19**, 186207 (2007).

[11] Ya. B. Burak, V. T. Adamiv, I. M. Teslyuk, and V. M. Shevel, Radiat. Meas. **38**, 681 (2004).

[12] F. P. Doty, I. Zwieback, and W. Ruderman, U.S. Patent 6,388,260 (2002).

[13] E. Seidland and W. Schwertführer, Atomkernenergie **11**, 155 (1996).

[14] D. S. McGregor, T. C. Unruh, and W. J. McNeil, Nucl. Instrum. Methods Phys. Res. A **591**, 530 (2008).

[15] J. Uher, S. Pospisil, V. Linhart, and M. Schieber, Appl. Phys. Lett. **90**, 124101 (2007).

[16] J. Li, R. Dahal, S. Majety, J. Y. Lin, and H. X. Jiang, Nucl. Instrum. Methods Phys. Res. A **654**, 417 (2011).

[17] Y. Kumashiro, J. Mater. Res. **5**, 2933 (1990).

[18] Y. Kumashiro, J. Solid State Chem. **133**, 314 (1997).

[19] J. C. Lund, F. Olschner, F. Ahmed, and K. S. Shah, Mater. Res. Soc. Symp. Proc. **162**, 601 (1990).

[20] T. P. Viles, B. A. Brunnett, H. Yoon, J. C. Lund, H. Hermon, D. Buchenauer, K. McCarty, M. Clifft, D. Dibble, and R. B. James, Mater. Res. Soc. Symp. Proc. **487**, 585 (1998).

[21] A. N. Caruso, R. B. Billa, S. Balaz, J. I. Brand, and P. A. Dowben, J. Phys.: Condens. Matter **16**, L139 (2004).

[22] B. W. Robertson, S. Adenwalla, A. Harken, P. Welsch, J. I. Brand, P. A. Dowben, and J. P. Claassen, Appl. Phys. Lett. **80**, 3644 (2003).

[23] B. W. Robertson, S. Adenwalla, A. Harken, P. Welsch, J. I. Brand, J. P. Claassen, N. M. Boag, and P. A. Dowben, Proc. SPIE **4785**, 226 (2002).

[24] S. Adenwalla, R. Billa, J. I. Brand, E. Day, M. J. Diaz, A. Harken, A. S. McMullen-Gunn, R. Padmanabhan, and B. W. Robertson, Proc. SPIE **5199**, 70 (2003).

[25] K. Osberg, N. Schemm, S. Balkir, J. I. Brand, S. Hallbeck, P. Dowben, and M. W. Hoffman, IEEE Sens. J. **6**, 1531 (2006).

[26] K. Osberg, N. Schemm, S. Balkir, J. I. Brand, S. Hallbeck, and P. Dowben, in: IEEE International Symposium on Circuits and Systems (ISCAS 2006) Proceedings, (IEEE, 2006), p. 1179.

[27] A. N. Caruso, P. A. Dowben, S. Balkir, N. Schemm, K. Osberg, R. W. Fairchild, O. B. Flores, S. Balaz, A. D. Harken, B. W. Robertson, and J. I. Brand, Mater. Sci. Eng. B **135**, 129 (2006).

[28] E. Day, M. J. Diaz, and S. Adenwalla, J. Phys. D, Appl. Phys. **39**, 2920 (2006).

[29] N. Hong, J. Mullins, K. Foreman, and S. Adenwalla, J. Phys. D, Appl. Phys. **43**, 275101 (2010).

[30] P. A. Dowben, O. Kizilkaya, J. Liu, B. Montag, K. Nelson, I. Sabirianov, and J. I. Brand, Mater. Lett. **63**, 72 (2009).

[31] J. Liu, G. Luo, W.-N. Mei, O. Kizilkaya, E. D. Shepherd, J. I. Brand, and P. A. Dowben, J. Phys. D, Appl. Phys. **43**, 085403 (2010).

[32] G. Luo, J. Lu, J. Liu, W.-N. Mei, and P. A. Dowben, Mater. Sci. Eng. B **175**, 1 (2010).

[33] M. Lemonnier, O. Collet, C. Depautex, J. M. Esteva, and D. Raoux, Nucl. Instrum. Methods A **152**, 109 (1978).

[34] T. M. Hayes and J. B. Boyce, in: Solid State Physics, Vol. 37 (Academic, New York, 1982), p. 173.

[35] V. T. Adamiv, Ya. B. Burak, I. V. Kityk, J. Kasperczyk, R. Smok, and M. Czerwinski, Opt. Mater. **8**, 207 (1997).

[36] Ya. V. Burak, Ya. O. Dovgyi, and I. V. Kityk, Solid State Phys. **31**, 275 (1989).

[37] J. A. Bearden and A. F. Burr, Rev. Mod. Phys. **39**, 125 (1967).

[38] J. H. Hubbell, in: 51st National Meeting of the Japanese Society of Radiological Technology (Nagoya, Japan, 1995).

[39] V. Maslyuk, M. Islam, and T. Bredow, Phys. Rev. B **72**, 125101 (2005).

[40] M. Islam, T. Bredow, and C. Minot, J. Phys. Chem. B **110**, 17518 (2006).

[41] M. Islam, V. Maslyuk, T. Bredow, and C. Minot, J. Phys. Chem. B **109**, 13597 (2005).

[42] D. Wooten, I. Ketsman, J. Xiao, Ya. B. Losovyj, J. Petrosky, J. McClory, Ya. V. Burak, V. T. Adamiv, J. M. Brown, and P. A. Dowben, Eur. Phys. J.: Appl. Phys. **52**, 31601 (2010).

[43] A. A. Ahmad, N. J. Ianno, P. G. Snyder, D. Welipitiya, D. Byun, and P. A. Dowben, J. Appl. Phys. **79**, 8643 (1996).

[44] S. Lee, J. Mazurowski, G. Ramseyer, and P. A. Dowben, J. Appl. Phys. **72**, 4925 (1992).

[45] G. Bunker, Introduction to XAFS: A Practical Guide to X-ray Absorption Fine Structure Spectroscopy (Cambridge University Press, Cambridge, 2010).

[46] N. Dimakis, T. Mion, and G. Bunker, J. Phys.: Conf. Ser. **190**, 012011 (2009).

[47] B. V. Padlyak, W. Wojtowicz, V. T. Adamiv, Ya. V. Burak, and I. M. Teslyuk, Acta Pol. A **117**, 122 (2010).

[48] B. V. Padlyak, A. Drzewiecki, and O. O. Smyrnov, Curr. Top. Biophys. **33**, 171 (2010).

[49] D. Podgórska, S. M. Kaczmarek, W. Drozdowski, W. Wabia, M. Kwasny, S. Warchoł, and V. M. Rizak, Mol. Phys. Rep. **39**, 199 (2004).

[50] M. Danilkin, I. Jaek, M. Kerikmäe, A. Lust, H. Mändar, L. Pung, A. Ratas, V. Seeman, S. Klimonsky, and V. Kuznetsov, Radiat. Meas. **45**, 562 (2010).

[51] V. M. Holovey, V. I. Lyamayev, M. M. Birov, P. P. Puga, and A. M. Solomon, Funct. Mater. **12**, 318 (2005).

[52] V. M. Holovey, V. I. Sidev, V. I. Lyamayev, and M. M. Birov, J. Phys. Chem. Solids **68**, 1305 (2007).

[53] A. Klemen, V. M. Holovey, and M. Ignatovich, Radiat. Meas. **43**, 375 (2008).

[54] A. T. Brant, B. E. Kananan, M. K. Murari, J. W. McClory, J. C. Petrosky, V. T. Adamiv, Ya. V. Burak, P. A. Dowben, and L. E. Halliburton, J. Appl. Phys. **110**, 093719 (2011).

[55] K. P. Popovych, P. P. Puga, V. T. Maslyuk, V. M. Krasylynec, V. M. Holovey, and G. D. Puga, Acta Phys. Pol. A **117**, 174 (2010).

[56] M. Danilkin, M. Kerikmäe, A. Kirillov, A. Lust, A. Ratas, L. Paama, and V. Seeman, Proc. Estonian Acad. Sci. Chem. **55**, 123 (2006).

[57] S. Kar, S. Verma, and K. S. Bartwal, Physica B **405**, 4299 (2010).

[58] M. Ignatovych, V. Holovey, T. Vidoczy, P. Baranyai, and A. Kelemen, Radiat. Phys. Chem. **76**, 1527 (2007).

[59] O. Annalakshmi, M. T. Jose, and G. Amarendra, Radiat. Meas. **46**, 669 (2011).